JOURNAL OF GEOPHYSICAL RESEARCH, VOL. 113, A11306, doi:10.1029/2008JA013114, 2008



# Solar activity variations of nighttime ionospheric peak electron density

Yiding Chen,[1,2] Libo Liu,[1] and Huijun Le[1,2]

Received 22 February 2008; revised 30 June 2008; accepted 18 August 2008; published 5 November 2008.

[1] Monthly median $N_mF_2$ (maximum electron density of the $F_2$-layer) data at Okinawa, Yamagawa, Kokubunji, and Wakkanai have been collected to investigate the solar activity dependence of the nighttime ionosphere. The result shows that there are seasonal and latitudinal differences of the solar activity variation of nighttime $N_mF_2$. The main seasonal effects are as follows: nighttime $N_mF_2$ increases with $F_{107}$ linearly in equinoctial months (March and September), and it tends to saturate with $F_{107}$ increasing in summer solstice month (June). What is peculiar is that there is an amplification trend of nighttime $N_mF_2$ with $F_{107}$ in winter solstice month (December). The latitudinal difference is mainly displayed by the evolvement course of the variation trend between $N_mF_2$ and $F_{107}$. Using $h_mF_2$ (peak height of the $F_2$-layer) data and the NRLMSISE00 model, we estimated the recombination loss around the $F_2$-peak at different solar activity levels. We found that the solar activity variation of the recombination processes around the $F_2$-peak also shows seasonal dependence, which can explain the variation trends of nighttime $N_mF_2$ with $F_{107}$ qualitatively, and field-aligned plasma influx plays an important role in the equatorial ionization anomaly (EIA) crest region. During the first several hours following sunset in December, there are faster recombination processes around the $F_2$-peak at medium solar activity level in mid-latitude regions. This feature is suggested to be responsible for inducing the amplification trend in winter. In virtue of the calculation of neutral parameters at 300-km altitude and $h_mF_2$ data, the variation trend of the recombination processes around the $F_2$-peak with $F_{107}$ can be explained. It shows that both the solar activity variations of $h_mF_2$ and neutral parameters (neutral temperature, density, and vibrational excited $N_2$) are important for the variation trend of nighttime $N_mF_2$ with $F_{107}$. Furthermore, the obvious uplift of $h_mF_2$ at low solar activity level following sunset in December is important for the amplification trend.

**Citation:** Chen, Y., L. Liu, and H. Le (2008), Solar activity variations of nighttime ionospheric peak electron density, *J. Geophys. Res.*, *113*, A11306, doi:10.1029/2008JA013114.

## 1. Introduction

[2] The Earth's ionosphere is mainly produced via the photoionization of the upper atmosphere by solar EUV and X-ray radiation. As a result, the behaviors of the ionosphere are strongly controlled by solar radiation. The variations of solar radiation are significant over different timescales, which of course will cause corresponding variations in the ionosphere [e.g., *Ivanov-Kholodny and Mikhailov*, 1986; *Kawamura et al.*, 2002; *Rishbeth and Garriott*, 1969]. The 11-year solar cycle variation is a prominent component of the variations of solar radiation [e.g., *Kane*, 1992, 2003; *Lean et al.*, 2001], which affects the ionosphere significantly. Therefore, the study about the solar activity variations of the ionosphere is essential for understanding the long-term variations of the ionosphere. Previous works about the solar activity dependence of the ionosphere mainly pay attention to the daytime ionosphere, which show complicated solar activity variations of the ionosphere [e.g., *Adler et al.*, 1997; *Balan et al.*, 1994a, 1994b, 1996; *Bilitza et al.*, 2007; *Gupta and Singh*, 2001; *Huang and Cheng*, 1995; *Kane*, 1992, 2003; *Kouris et al.*, 1998; *Lei et al.*, 2005; *Liu et al.*, 2003, 2004, 2006, 2007a, 2007b; *Mikhailov and Mikhailov*, 1995; *Richards*, 2001; *Sethi et al.*, 2002; *Su et al.*, 1999].

[3] Recent works show there is a nonlinear relation between daytime ionospheric parameters ($N_mF_2$, maximum electron density of the $F_2$-layer; $f_oF_2$, critical frequency at the $F_2$-peak; *TEC*, total electron content) and solar proxies (such as $F_{107}$, 10.7 cm solar radiation flux) in all seasons. The ionospheric parameters approximately increase linearly with solar proxies at low and medium solar activity levels; however they tend to saturate at high solar activity level [e.g., *Balan et al.*, 1994a, 1994b, 1996; *Gupta and Singh*, 2001; *Lei et al.*, 2005; *Liu et al.*, 2003, 2004, 2006; *Richards*, 2001; *Sethi et al.*, 2002; *Su et al.*, 1999]. *Balan et al.* [1994a, 1994b, 1996] proposed that the saturation effect during daytime is due to the nonlinear variations of

[1]Beijing National Observatory of Space Environment, Institute of Geology and Geophysics, Chinese Academy of Sciences, Beijing, China.
[2]Graduate University of Chinese Academy of Sciences, Beijing, China.


0148-0227/08/2008JA013114$09.00

**Table 1.** Information of the Ionosonde Stations Used in Our Work

| | Geographic Coordinate | | Geomagnetic Parameters | | |
|---|---|---|---|---|---|
| Station Name | Latitude | Longitude | Latitude | Dip | Year Segments of Data |
| Okinawa | 26.3 | 127.8 | 15.8 | 36.6 | 1957–1989, 1992–1993, and 1996–2007 |
| Yamagawa | 31.2 | 130.6 | 20.8 | 44.0 | 1957–1988, 1996–1999, and 2001–2007 |
| Kokubunji | 35.7 | 139.5 | 25.9 | 48.8 | 1957–2007 |
| Wakkanai | 45.4 | 141.7 | 35.8 | 59.5 | 1948–1988, 1992–1993, and 1996–2007 |

solar EUV flux with $F_{107}$, while $N_mF_2$ and *TEC* increase linearly with integrated EUV flux. *Liu et al.* [2003] found that the saturation effect also exists between $f_oF_2$ and solar EUV radiation, and the most profound saturation effect occurs in the equatorial ionization anomaly (EIA) region. They supposed that the daily equatorial fountain effect and the prereversal enhancement are important for the saturation. Recently, *Liu et al.* [2006] systematically investigated the dependence of noontime $N_mF_2$ with solar EUV flux in the East Asia/Australia sector. Their result shows a significant saturation effect between $N_mF_2$ and EUV flux at low latitudes, which also confirms that the saturation effect between $N_mF_2$ and $F_{107}$ cannot only be attributed to the nonlinear increase of EUV flux with $F_{107}$. They showed that the ionospheric dynamics and the variations of neutral atmosphere also play important roles. Furthermore, some works about the solar activity dependence of the topside ionosphere have been carried out recently [e.g., *Liu et al.*, 2007a, 2007b]. The results show that the solar activity dependence of the topside ionosphere is quite different from that in the $F_2$-layer, which further indicates the importance of the ionospheric dynamics for the solar activity dependence of the ionosphere.

[4] Previous works are rarely concentrated on the solar activity effects of the nighttime ionospheric electron density. Different from the situation for the daytime ionosphere, photoionization processes can be neglected in the F-region during nighttime. The electron density at any given moment largely depends on its historical values. So the nighttime ionosphere cannot be treated independently. Recombination processes and the ionospheric dynamics simultaneously control the evolvement of the nighttime ionosphere. On the one hand, ionospheric dynamics processes directly affect the nighttime electron density. Downward field-aligned plasma influx can maintain the nighttime $F_2$-layer to some extent, and its contribution is prominent when it is comparable with recombination processes [e.g., *Mikhailov et al.*, 2000]. On the other hand, the ionospheric dynamics strongly affects recombination processes by changing the altitudes of the ionosphere. The $F_2$-layer is uplifted to higher altitudes during nighttime by the upward plasma drift caused by equatorward neutral winds. That strongly affects the recombination processes in the F-region. Therefore, the nighttime ionosphere may be more sensitive to the ionospheric dynamics. From another point of view, the study about the solar activity variations of the nighttime ionosphere should be more suitable for investigating the effects of the ionospheric dynamics. *Liu et al.* [2004] investigated the variations of nighttime $f_oF_2$ with $F_{107}$ using Wuhan ionosonde observations. They showed seasonal difference of the solar activity dependence of nighttime $f_oF_2$. However we do not know whether this seasonal difference is a general effect, and the possible mechanism is not discussed as well. All these form the motivation of this study.

[5] This work investigates the solar activity dependence of nighttime $N_mF_2$ in different seasons and latitudes. The purposes of this work are twofold: (1) to investigate the solar activity dependence of nighttime $N_mF_2$ and its seasonal and latitudinal variations; and (2) to evaluate the solar activity variations of upper atmosphere and the ionospheric dynamics, and to discuss their contributions to the solar activity variation of nighttime $N_mF_2$.

## 2. Data

[6] Data from various ionosonde stations have been accumulated over a long time, which is essential for investigating the solar activity dependence of the ionosphere. In this work, four ionosonde stations' data for several solar cycles were collected to study the solar activity dependence of the nighttime ionosphere. The stations we analyzed are located in the East Asia/Australia sector, with geographic latitudes spanning from 26.3°N to 45.4°N (see Table 1). Hourly values of $f_oF_2$, $f_oE$ (critical frequency of the E-layer) and $M(3000)F_2$ (maximum usable frequency factor) are provided by NICT (National Institute of Information and Communications Technology). We adopt the adjusted $F_{107}$ as solar proxy, which is provided at the SPIDR website.

[7] Monthly median values of ionospheric parameters can represent the average behavior of the ionosphere well. We adopt monthly median $f_oF_2$ and $F_{107}$ in this work. The data will be discarded if the count number in one month at any given local time is less than 10. Monthly median $N_mF_2$ are derived from monthly median $f_oF_2$ data. Monthly median $h_mF_2$ (peak height of the $F_2$-layer) are calculated in terms of monthly median $f_oF_2$, $f_oE$ and $M(3000)F_2$ according to *Dudeney* [1983]. In order to investigate the seasonal variation of the solar activity dependence of the nighttime ionosphere,

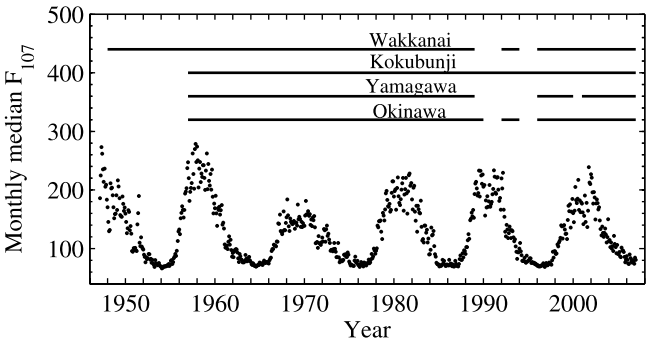


**Figure 1.** The monthly median $F_{107}$ (in unit of $10^{-22}$ W · m$^{-2}$ · Hz$^{-1}$). Horizontal solid lines represent the time coverage of ionosonde data.

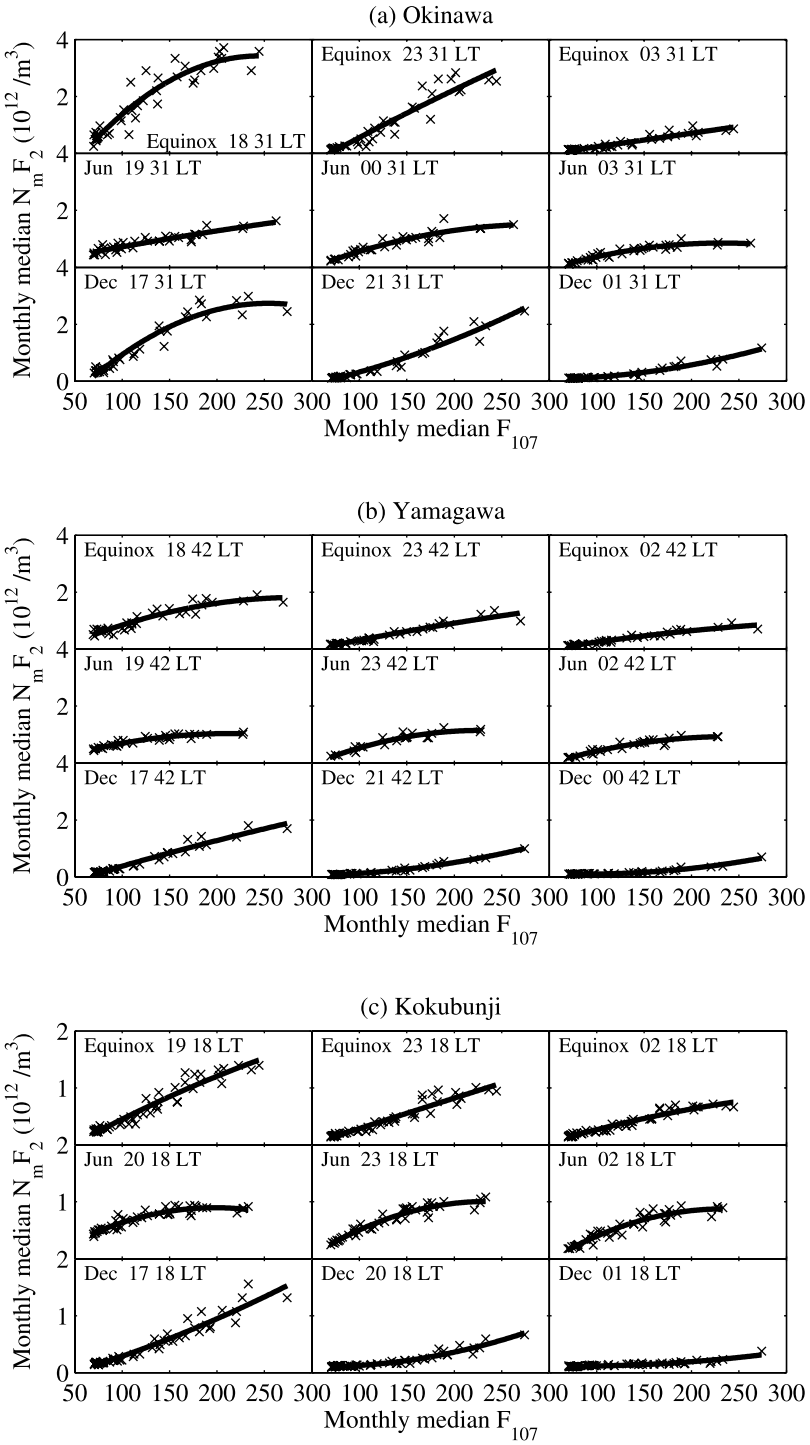


**Figure 2.** Variations of nighttime $N_mF_2$ (in unit of $10^{12}$ electrons/m$^3$) with $F_{107}$ (in unit of $10^{-22}$ W · m$^{-2}$ · Hz$^{-1}$) at (a) Okinawa, (b) Yamagawa, (c) Kokubunji, and (d) Wakkanai. $N_mF_2$ and $F_{107}$ are monthly median values. Equinox, Jun, and Dec represent equinoctial months, June, and December, respectively, and three mass plots at different local times show the evolvement of the solar activity dependence. The crosses represent observations, and the solid curves are quadratic regression fits.

we selectively analyzed the data of March, June, September, and December, which stand for spring, summer, autumn, and winter respectively. Figure 1 shows the solar cycle variation of monthly median $F_{107}$, as well as the time coverage of the ionosonde data used in this work.

## 3. Results

[8] Figure 2 presents the solar activity variations of nighttime $N_mF_2$ at Okinawa, Yamagawa, Kokubunji, and Wakkanai. The crosses are monthly median values of observed ($N_mF_2$, $F_{107}$), and the solid curves denote quadratic regression fits between $N_mF_2$ and $F_{107}$. The data in

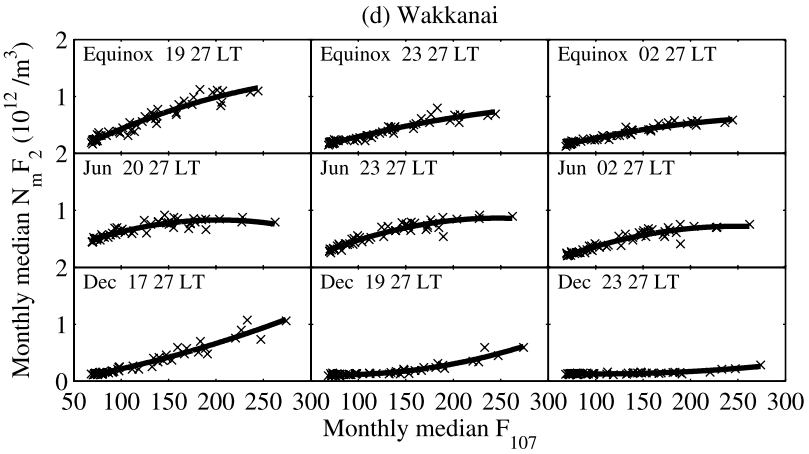


**Figure 2.** (continued)

March show a similar variation trend as that in September, therefore, we combine these two months data as Equinox. The result shows that there is an obvious seasonal difference in the relationship between nighttime $N_mF_2$ and $F_{107}$, which differs from the saturation effect during daytime in all seasons [e.g., *Balan et al.*, 1994a, 1996; *Gupta and Singh*, 2001; *Liu et al.*, 2004, 2006; *Richards*, 2001; *Sethi et al.*, 2002]. Several hours later after sunset (Table 2 gives corresponding mean local time when the solar zenith equals to 90 degrees at ground dusk), which depends on latitude, $N_mF_2$ appears different variation trends with $F_{107}$. Nighttime $N_mF_2$ approximately increases linearly with $F_{107}$ in equinoctial months, and it tends to saturate when $F_{107}$ exceeds a threshold in June. What is peculiar is that there is an amplification trend of nighttime $N_mF_2$ when $F_{107}$ increases in December. That is contrary to the daytime saturation effect.

[9] Since the nighttime ionosphere largely depends on its historical state, it's necessary for us to know how the relation between nighttime $N_mF_2$ and $F_{107}$ evolves with local time. We selected three representative cases, which are at local times distributing from sunset to post-midnight, to show the evolvement process in every month. There are latitudinal differences of the evolvement process in all seasons. (1) The daytime saturation effect continues for about one hour following sunset, before it tends toward linear increase gradually, at low latitude stations (Okinawa and Yamagawa) in equinoctial months. While at mid-latitude stations (Kokubunji and Wakkanai), the linear increase trend between $N_mF_2$ and $F_{107}$ establishes quickly following sunset in equinoctial months. (2) $N_mF_2$ tends to saturate with $F_{107}$ increasing during nighttime in June except at Okinawa, where $N_mF_2$ increases linearly with $F_{107}$ around sunset before it tends to saturate gradually. (3) $N_mF_2$ saturates with $F_{107}$ around sunset at Okinawa in December, and the amplification trend is visible about four hours later. While $N_mF_2$ approximately increases with $F_{107}$ linearly for about one hour following sunset at the other stations in December, and then it tends toward an amplification trend quickly.

[10] The latitudinal features of the solar activity variation in December are analyzed except for what we referred above for the particular solar activity variation of nighttime $N_mF_2$ in winter. Figure 3 presents $F_{107}$ and local time variations of nighttime $N_mF_2$ at four ionosonde stations in December. The $N_mF_2$ data at different local times are quadratic regression fitted values between $N_mF_2$ and $F_{107}$. Figure 3 shows that $N_mF_2$ attenuates obviously with local time throughout all night at Okinawa, especially at high solar activity level. While $N_mF_2$ just decreases rapidly with local time during about the first four hours following sunset at Wakkanai, and then it changes little until dawn. At Yamagawa and Kokubunji, the cases transit gradually. The modalities of $N_mF_2$ with $F_{107}$ at different local times also vary with latitude. The feature of the amplification trend of $N_mF_2$ with $F_{107}$ keeps obviously until dawn at Okinawa. But with latitude increasing, there is only weak increase of $N_mF_2$ with $F_{107}$ after midnight at Wakkanai. Moreover, it is noticeable that $N_mF_2$ only changes little and steadies at higher levels between 1830 LT and 2030 LT at Okinawa.

## 4. Discussion

[11] Recombination processes and the ionospheric dynamics simultaneously control the variations of the nighttime ionosphere. The ionospheric dynamics processes mainly involve drifts caused by neutral winds and electric fields, field-aligned plasma influx, diffusion as well as thermal expansion and contraction. Diffusion process is more important in the topside ionosphere except in magnetic equatorial region due to the exponential decrease of ion-neutral collision frequency with altitude, while it is

**Table 2.** Local Time When the Solar Zenith Equals to 90° at Dusk[a]

| | Local Time | | | |
|---|---|---|---|---|
| Station Name | March | June | September | December |
| Okinawa | 17:59 | 18:49 | 18:03 | 17:11 |
| Yamagawa | 17:59 | 19:01 | 18:04 | 16:59 |
| Kokubunji | 17:59 | 19:13 | 18:04 | 16:48 |
| Wakkanai | 17:58 | 19:44 | 18:06 | 16:16 |

[a]March, June, September, and December are corresponding to 80th, 170th, 260th, and 350th day, respectively.

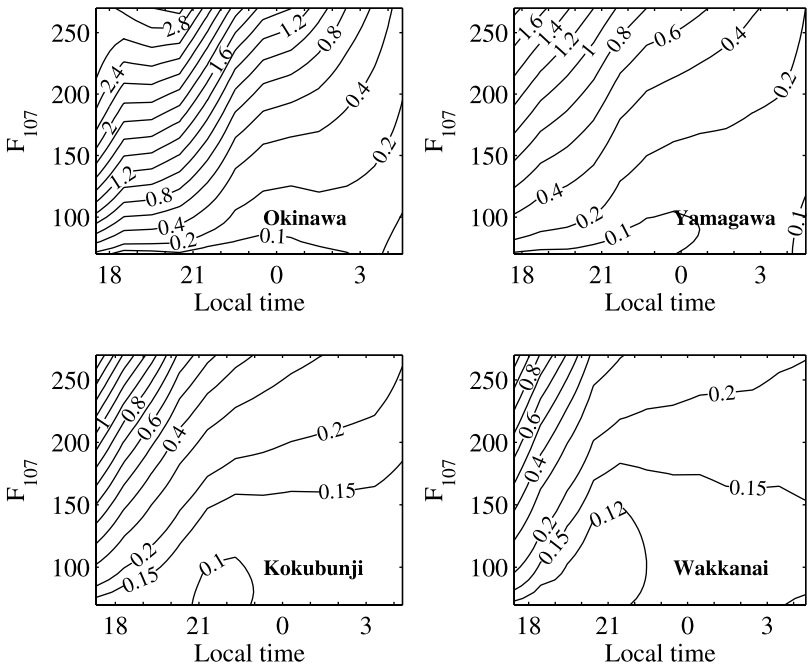


**Figure 3.** The variations of nighttime $N_mF_2$ (in unit of $10^{12}$ electrons/m$^3$) with local time and $F_{107}$ (in unit of $10^{-22}$ W·m$^{-2}$·Hz$^{-1}$) at Okinawa, Yamagawa, Kokubunji, and Wakkanai in December. The $N_mF_2$ data with $F_{107}$ of different local times are quadratic regression fitted values.

weak around the $F_2$-peak for little plasma gradient [*Rishbeth*, 1986]. Here we will not pay more attention to diffusion process.

[12] Drifts and thermal contraction mainly contribute to the change of $h_mF_2$ during nighttime. They, together with the variations of background atmosphere, affect the recombination loss around the $F_2$-peak. We introduce $\beta_m$ to describe the recombination rate at the peak height of the $F_2$-layer. $\beta_m$ depends on $h_mF_2$ and the state of background atmosphere, so the variation of $\beta_m$ includes the effects caused by the variations of background atmosphere and also the ionospheric dynamics that induce the movement of the $F_2$-peak. Field-aligned plasma flux is downward during nighttime. It can maintain the $F_2$-peak significantly when recombination loss is relatively small. Prereversal enhancement of the vertical drift induced by the eastern electric field raises the ionosphere to higher altitudes in magnetic equatorial region, and subsequently the plasma diffuses to both hemispheres along magnetic field lines. That causes great field-aligned plasma influx in EIA crest region [e.g., *Rishbeth and Garriott*, 1969]. Therefore, field-aligned influx is important for the nighttime ionosphere in EIA crest region when the prereversal enhancement is taking effect.

[13] In this paper, we estimated $N_mF_2$ based on the recombination processes around the $F_2$-peak in order to evaluate the importance of recombination loss around the $F_2$-peak, which contains the effects of chemical and dynamic processes that induce the change of $h_mF_2$, and field-aligned plasma influx for causing solar activity variations of nighttime $N_mF_2$. By doing so, the effect of field-aligned influx can be distinguished from that of other dynamic processes that cause the change of $h_mF_2$. The calculations are carried out during an hour interval with a time step of one minute by following continuity equation which only recombination processes around the $F_2$-peak are included in.

$$\frac{\partial N_mF_2}{\partial t} = -N_mF_2 \times \beta_m \tag{1}$$

We adopt fitted values between monthly median $h_mF_2$ and $F_{107}$ to calculate $\beta_m$ ($\beta_m$ with one minute step is estimated by interpolation with observed hourly $h_mF_2$ data). Neutral parameters and ionic temperature are calculated using the NRLMSISE00 model [*Picone et al.*, 2002] and the IRI2000 model [*Bilitza*, 2001].

[14] The ion $O^+$ is the dominant positive ion in the $F_2$ region [*Rishbeth and Garriott*, 1969], so only the recombination process of $O^+$ is included when we calculate $\beta_m$. Two main chemical reactions which cause the loss of $O^+$ are listed in Table 3. Where $N_2$* is vibrational excited $N_2$, which is important in the $F_2$ region by increasing the recombination rate of $O^+$ [e.g., *Pavlov*, 1994; *Pavlov and Buonsanto*, 1996; *Richards and Torr*, 1986]. We just include the effect of vibrational quanta $\nu = 0 \sim 5$. Here we introduce a parameter $\gamma$ to describe the effect of vibrational excited nitrogen on recombination process

$$\gamma = \frac{1}{[N_2]}\Big([N_2(\nu=0)] + [N_2(\nu=1)] + [N_2(\nu=2)] \times 38 + [N_2(\nu=3)] \times 85 + [N_2(\nu=4)] \times 220 + [N_2(\nu=5)] \times 270\Big) \tag{2}$$

$$k_1 = \gamma \cdot k_{10}$$

So $\gamma$ is the equivalent coefficient of ground state $N_2$ ($N_2(\nu = 0)$). Namely, the contribution of $N_2$ with a

**Table 3.** The Reactions Between $O^+$ and Dominant Neutral Molecules

| Reaction | Reaction Coefficient ($m^3\ s^{-1}$) |
|---|---|
| $O^+ (^4s) + N_2^* (\nu) \rightarrow NO^+ + N$ | $k_{10} = \left[1.533 - 0.592 \times \frac{T_{eff}}{300} + 0.086 \times \left(\frac{T_{eff}}{300}\right)^2\right] \times 10^{-18}$ |
| [*St. Maurice and Torr*, 1978] | $300\ K \leq T_{eff} \leq 1700\ K$ |
| | $k_{10} = \left[2.73 - 1.155 \times \frac{T_{eff}}{300} + 0.1483 \times \left(\frac{T_{eff}}{300}\right)^2\right] \times 10^{-18}$ |
| | $1700\ K < T_{eff} < 6000\ K$ |
| | $k_{11} = k_{10}$<br>$k_{12} = 38k_{10}$<br>$k_{13} = 85k_{10} \quad k_1 = \sum_{\nu=0}^{5} k_{1\nu} \times \frac{[N_2^*(\nu)]}{[N_2]}$<br>$k_{14} = 220k_{10}$<br>$k_{15} = 270k_{10}$ |
| $O^+ + O_2 \rightarrow O_2^+ + O$ | $k_2 = \left[17 \times \left(\frac{300}{T_n}\right)^{0.77} + 85.4 \times \exp(-3467/T_n)\right] \times 10^{-18}$ |
| [*Hierl et al.*, 1997] | |

density $[N_2]$, which contains different vibrational excited $N_2$, to recombination process is equivalent to the contribution of ground state $N_2$ with a density $\gamma[N_2]$. $T_{eff}$ is effective temperature, given by

$$T_{eff} = \frac{m_i T_n + m_n T_i}{m_i + m_n} \tag{3}$$

$m_i$ and $m_n$ are the masses of ions and neutral molecules respectively, and $T_i$ and $T_n$ are corresponding to the temperatures of ions and neutral atmosphere.

[15] Field-aligned plasma influx is important for the ionosphere in EIA crest region because of the fountain effect. Okinawa station is located in EIA crest region. Prereversal enhancement of E × B drift induces strong fountain effect. So estimations are investigated for Okinawa at times when the prereversal enhancement is taking effect, and at midnight when the prereversal enhancement has faded away. Meanwhile, the estimations of Wakkanai are investigated for the situation in mid-latitudes. The results are shown in Figure 4. Dashed lines are quadratic regression fits between $N_mF_2$ and $F_{107}$ at the local time one hour before the time labeled in each panel, which are adopted as the initial conditions for our calculation. Solid lines and circles are the estimated values and the observations at the time labeled in every panel respectively.

[16] For Okinawa, estimated values (solid lines) are coincident with observations (circles) at low solar activity level in equinoctial months and December when the prereversal enhancement is taking effect (the first row in Figure 4); but observations are greater than estimated values, even $N_mF_2$ increase with local time in equinoctial months (Equinox 1931 LT, circles and dashed line), at high solar activity level. Meanwhile, obvious decrease of $N_mF_2$ is observed in June when the prereversal enhancement is taking effect. Prereversal enhancement induces great field-aligned plasma influx at Okinawa. There are obvious seasonal and solar activity dependences in the prereversal enhancement of E × B drift. Prereversal enhancement of E × B drift is strong in equinoctial seasons and weak in summer, and it enhances with solar activity [e.g., *Fejer*, 1981; *Fejer et al.*, 1979, 1991, 1995; *Scherliess and Fejer*, 1999; *Whalen*, 2004]. Furthermore, the position of the EIA crest changes according to the strength of

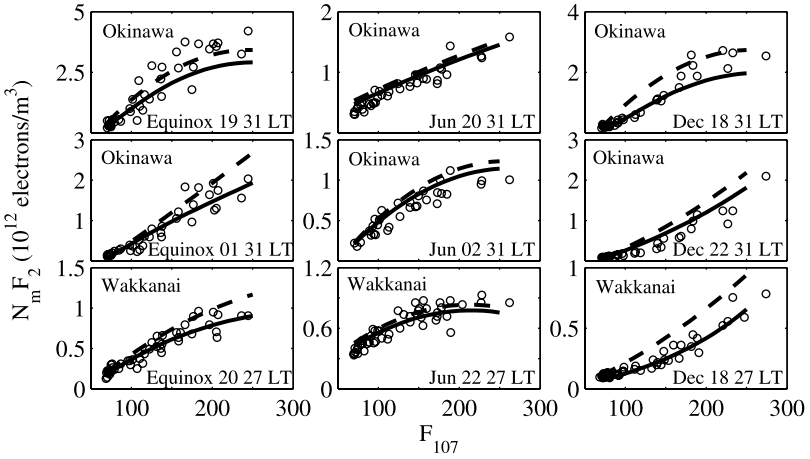


**Figure 4.** The estimation of $N_mF_2$ by the recombination rate at the peak height of the $F_2$-layer. Circles are observed monthly median ($N_mF_2$, $F_{107}$), and solid lines are estimated $N_mF_2$ at different $F_{107}$. Dashed lines represent quadratic regression fits between $N_mF_2$, which are observed values at the time 1 hour before the time labeled in each panel, and $F_{107}$. These fitted values are adopted as the initial conditions for estimation.

the E × B drift [e.g., *Liu et al.*, 2007b]. There is most prominent enhancement of electron density in the central region of the crest. Okinawa is possibly not located in the central region of EIA crest at low solar activity level and in summer for lesser crest-to-crest width. $N_mF_2$ saturates with $F_{107}$ increasing around sunset at Okinawa in equinoctial months and December. Recombination loss around the $F_2$-peak (it contains the effects of chemical and dynamic processes that induces the change of $h_mF_2$) is more significant than the contribution of field-aligned influx at low solar activity level in equinoctial months and December; while field-aligned influx comes to such great values that its contribution to $N_mF_2$ is comparable with the recombination loss around the $F_2$-peak, or it even dominants over the recombination loss around the $F_2$-peak in equinoctial months, at high solar activity level. So $N_mF_2$ decreases with local time at low solar activity level when the prereversal enhancement is taking effect in equinoctial months and December; while it keeps at some higher values, or it even increases with local time, at higher solar activity levels. As a result, $N_mF_2$ has a linear increase trend with $F_{107}$ when we organize the data by local time. Moreover, we notice that $N_mF_2$ only changes little during the period between 1830 LT and 2030 LT at Okinawa (Figure 3). That also should be contributed to the maintenance of field-aligned plasma influx. Field-aligned influx is less at Okinawa in summer for weaker prereversal enhancement. Observations indicate recombination loss around the $F_2$-peak is dominant in June.

[17] The estimations for midnight situation show that recombination loss around the $F_2$-peak is the main factor controlling the variation of nighttime $N_mF_2$ at Okinawa when the prereversal enhancement has faded away. Prereversal enhancement results in the linear increase trend of $N_mF_2$ with $F_{107}$ in December, while an amplification trend establishes gradually several hours later. We investigated the variation of $\beta_m$ with $F_{107}$ (Figure 5) and found that there are greater $\beta_m$ at medium solar activity level in December. That should cause quicker recombination processes at medium solar activity level. As a result, $N_mF_2$ has an amplification trend with $F_{107}$ when we organize the data by local time. Estimations of Wakkanai also indicate that the variation of $N_mF_2$ is mainly controlled by the recombination loss around the $F_2$-peak. Especially in December, $N_mF_2$ decrease quickly with local time at medium solar activity level because of the great $\beta_m$ values (Figure 5). So an amplification trend between $N_mF_2$ and $F_{107}$ establishes gradually. Furthermore, prereversal enhancement induces high $N_mF_2$ at Okinawa in winter, thus $N_mF_2$ attenuates obviously with local time and the amplification trend keeps throughout all night; while $N_mF_2$ attenuates to lower values quickly at Wakkanai in winter, and it remains at some background levels after midnight (see Figure 3) since the topside plasma supplies the little recombination loss [e.g., *Ivanov-Kholodny and Mikhailov*, 1986; *Rishbeth and Garriott*, 1969].

[18] The nighttime ionosphere depends on its historical state. There are linear increase trend of $N_mF_2$ with $F_{107}$ in equinoctial months and December, but different trends develop (linear trend in equinoctial months and amplification trend in December) under the control of recombination processes around the $F_2$-peak. On the one hand, the variations of neutral parameters directly affect recombination rate; on the other hand, the peak height of the $F_2$-layer is changed because of the change of neutral winds and the contraction of thermospheric atmosphere [*Rishbeth*, 1986]. Therefore, we analyze the question by these two aspects infra.

[19] We investigated the influence of the solar activity variations of neutral parameters on recombination processes. The chemical reaction between $N_2$ and $O^+$ is the primary one that caused the recombination loss of $O^+$. We make following discussions based on this reaction. Neutral temperature varies little with altitude in the $F_2$ region. We may postulate it is isothermal in the $F_2$-region. Then the density of each neutral composition attenuates with altitude exponentially with a fixed scale height. Another important parameter is $\gamma$ (equivalent coefficient of ground state $N_2$). We calculated the altitudinal variation of $\gamma$ at different solar activity levels by Pavlov's model [*Pavlov*, 1998] and found that there is little altitudinal variation at altitudes above 250 km where the $F_2$-peak stays during nighttime. Therefore we may assume that recombination rate caused by $N_2$ decreases exponentially with altitude. We choose 300 km as a reference height. The recombination rate caused by $N_2$ at $h_mF_2$ can be expressed approximately as follows

$$\beta_m = \beta_{300} \times \exp\left(-\frac{h_mF_2 - 300}{H}\right) \tag{4}$$

Where $\beta_{300}$ is the recombination rate caused by $N_2$ at an altitude of 300 km, and $H$ is the scale height of $N_2$. We get equation (5) by differentiating equation (4) with $F_{107}$.

$$\frac{\partial \beta_m}{\partial F_{107}} = \left\{\frac{\partial \beta_{300}}{\partial F_{107}} - \frac{\beta_{300}}{H^2} \times \left[H \times \frac{\partial h_mF_2}{\partial F_{107}} - (h_mF_2 - 300) \times \frac{\partial H}{\partial F_{107}}\right]\right\} \times \exp\left(-\frac{h_mF_2 - 300}{H}\right) \tag{5}$$

The bottom-middle panel of Figure 5 is calculated by equation (5), which shows the variation trend of $\beta_m$ with $F_{107}$.

[20] We discuss the effects of neutral temperature and density respectively by equation (5), though actually density is controlled by temperature to some extent. Here the effect of these two parameters on $h_mF_2$ does not take into account. The effect of neutral density can be presented by $\beta_{300}$. Neutral temperature affects $\beta_{300}$ and scale height simultaneously. $T_n$, $[N_2]$ and $h_mF_2$ all increase with $F_{107}$. So $\beta_{300}$ increases with $F_{107}$ because of the increase of $T_n$ and $[N_2]$. Meanwhile, scale height increases with $F_{107}$ for the increase of $T_n$. That induces the decrease of altitudinal variation rate of recombination rate. Therefore, the increase of $T_n$ and $[N_2]$ induces the increase of recombination rate at different fixed heights, and the increase enhances with altitude increasing. The increase of $h_mF_2$ with $F_{107}$ should result in the decrease of $\beta_m$ if the background atmosphere does not change, while recombination rate also increases with $F_{107}$ at any fixed height because of the change of the background atmosphere. That counteracts the decrease of $\beta_m$ induced by the increase of $h_mF_2$ to a certain extent. So these two factors produce contrary effects on the change of $\beta_m$ with $F_{107}$, and the variation trend of $\beta_m$ with $F_{107}$ depends on the relative intensity of these two factors. The variation rates of neutral parameters and $h_mF_2$ with $F_{107}$ differ in different seasons. We discuss the variation trend of $\beta_m$ with $F_{107}$ by these

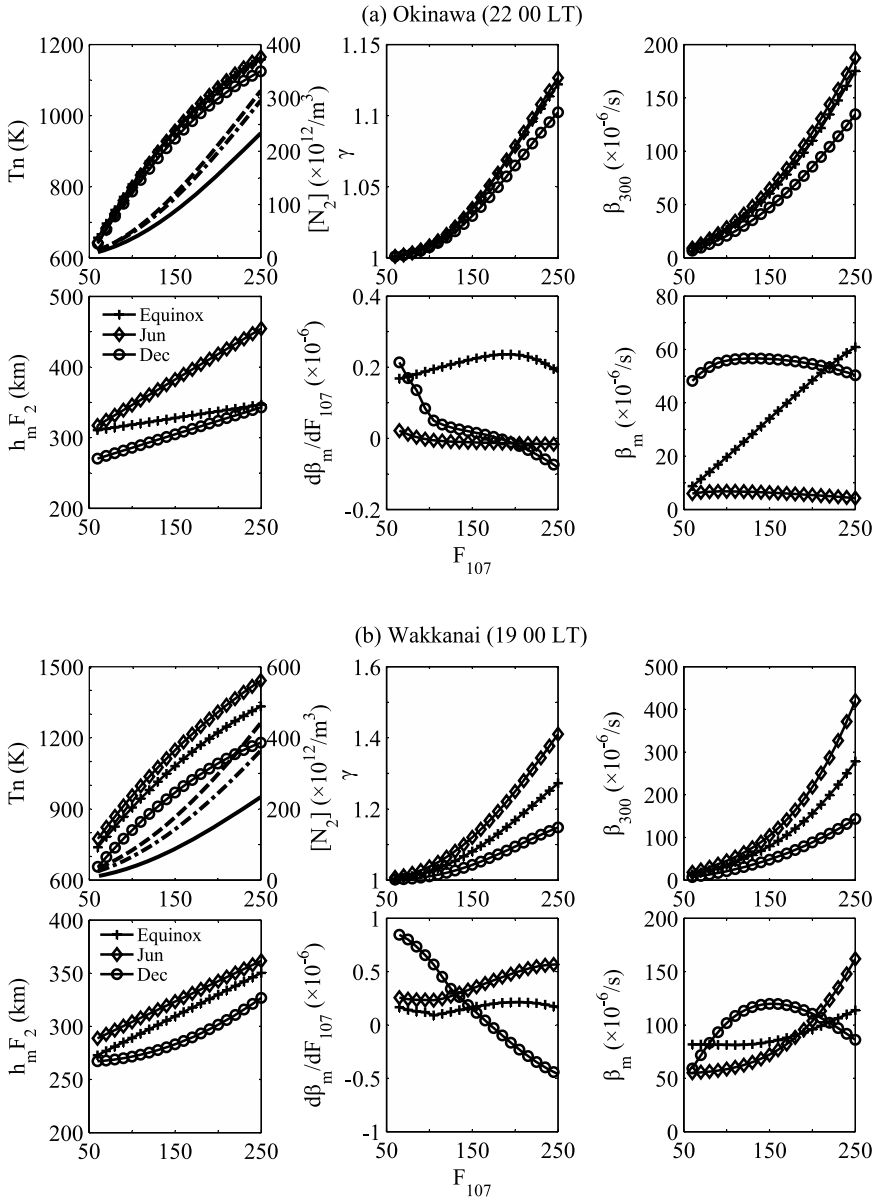


**Figure 5.** Calculated $T_n$ (neutral temperature), [$N_2$] (nitrogen density; lines without markers in the upper left panel; dashed line, dash–dot line and solid line are for June, Equinox, and December, respectively), $\gamma$ (equivalent coefficient of $N_2(\nu = 0)$) and $\beta_{300}$ (recombination rate) at an altitude of 300 km, and interpolated $h_mF_2$ from observations. $d\beta_m/dF_{107}$ shows the variation trend of the calculated recombination rate around the $F_2$-peak with $F_{107}$.

seasonal differences. As an example, we analyze the case at Wakkanai.

[21] Figure 5 shows the values of neutral parameters calculated by the NRLMSISE00 model. It shows that neutral temperature and density as well as their increase rates with $F_{107}$ are higher in June and equinoctial months than that in December. Therefore, the increase of $\beta_{300}$ with $F_{107}$ is more significant in June than that in December, especially at higher solar activity level. Another important parameter is the equivalent coefficient of ground state $N_2$. The upper-middle panel of Figure 5b also shows that the increase rate of $\gamma$ with $F_{107}$ is greater in June than that in December. This enhances the sharp increase of recombination rate with $F_{107}$ in June. It can be concluded that recombination rates increase with $F_{107}$ more intensively at higher altitudes. While $h_mF_2$ increases with a constant slope in June, and the $F_2$-peak always stays at higher altitudes. So the increase of recombination rate is more significant in June, namely $\beta_m$ increases with $F_{107}$. The case is different in December. The increase of $\beta_{300}$ is much slower as compared with that in June, while the increase of $h_mF_2$ is more and more rapid and the slope at high solar activity level is comparable with that in June. Thus the increase of recombination rate is more significant at low solar activity level in December for low increase rate of $h_mF_2$, while the increase of $h_mF_2$ is more significant at high solar activity level ($\beta_m$ decreases with $F_{107}$). The curve of $d\beta_m/dF_{107}$ shows this variation trend. There

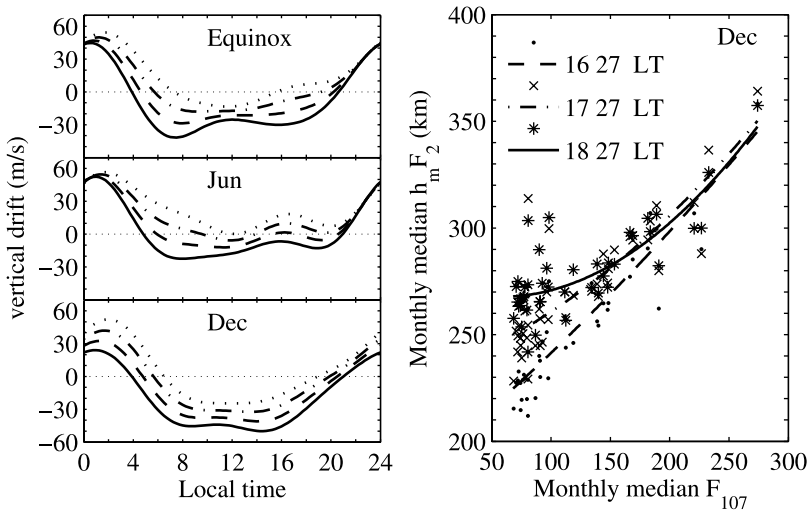


**Figure 6.** (left) Diurnal variations of the vertical drift at an altitude of 300 km caused by neutral winds at Wakkanai (upward positive). Dotted lines, dash−dot lines, dashed lines, and solid lines represent the values of vertical drifts at different solar activity levels for $F_{107}$ equals to 60, 120, 180, and 240, respectively. (right) The $F_{107}$ dependence of $h_mF_2$ in December. Dots denote observations, and lines are corresponding quadratic regression fits.

are larger values of $\beta_m$ at medium solar activity level. That causes quicker recombination processes. As a result, $N_mF_2$ has an amplification trend with $F_{107}$ when we organize the data by local time. There is a similar variation in equinoctial months with that in June.

[22] The peak height of the $F_2$-layer is strongly controlled by neutral winds [e.g., *Buonsanto*, 1990; *Rishbeth*, 1993]. Figure 6 shows the increase of $h_mF_2$ at Wakkanai induced by the transition of neutral winds. Figure 6 (left) is the vertical drift caused by neutral winds in equinoctial months, June and December (corresponding to 80th, 170th and 350th day respectively in calculations), which is calculated as follows:

$$W = -\frac{\Omega^2}{\Omega^2 + \nu^2}(u \cdot \sin D + v \cdot \cos D)\sin I \cos I \qquad (6)$$

Here $\Omega$ is the ionic gyrofrequency, and $\nu$ is the collision frequency between ions and neutral particles. $\Omega \gg \nu$ is valid in the $F_2$-region, so the first term equals to one approximately. $u$ and $v$ are the eastern and northern components of neutral winds respectively, which are calculated by the HWM93 model [*Hedin et al.*, 1996]. $D$ and $I$ are the declination angle and dip angle of the Earth's magnetic field respectively.

[23] Figure 6 (right) shows that the $F_2$-peak moves upward obviously at low solar activity level, while there is no obvious change at high solar activity level. There is a transition of the vertical drift from downward (daytime) to upward (nighttime) because of the change of neutral winds. The transition occurs during about 2∼4 hours following sunset (it occurs earlier at low solar activity level than that at high solar activity level) in December. According to the servo theory, the weakening of downward drift will cause the uplift of the $F_2$-peak [*Rishbeth et al.*, 1978], and the uplift effect is greater if downward drift is weaker. The downward drift has attenuated to low values at low solar activity level when it still remains at higher values at medium and high solar activity levels just following sunset in December. Thus, the weakening drift, as shown in Figure 6 (left) before the transition of meridional wind direction, produces greater uplift at low solar activity level than that at high solar activity level. In addition to the influence of vertical drift, the contraction of the thermospheric atmosphere will cause the drop of the $F_2$-layer peak, which counteracts the uplift partially. There is no obvious uplift at high solar activity level. A possible reason is that the contraction of thermosphere counteracts the weaker uplift caused by the transition course.

[24] Recombination rate attenuates exponentially with the reduced height approximately. The obvious increase of $h_mF_2$ causes sharp decrease of $\beta_m$ at low solar activity level in December. While as aforementioned discussion about neutral parameters, $\beta_m$ still presents negative correlation with $F_{107}$ at high solar activity level. So there are quicker recombination processes around the $F_2$-peak at medium solar activity level to cause the amplification trend. The reversal of vertical drift also occurs in equinoctial months and June, and it also causes the uplift of the $F_2$-peak. Different from that in December, the reversal course occurs before or around sunset at low and medium solar activity levels, and it has developed much around sunset (especially in June). Thus the uplift of $h_mF_2$ occurs at different solar activity levels, and the increase rate of $h_mF_2$ with $F_{107}$ does not differ greatly at different solar activity levels as that in December.

## 5. Summary

[25] We investigated the solar activity dependence of nighttime $N_mF_2$ using the long-term observations at four ionosonde stations. The results show obvious seasonal differences. The different variation trends of nighttime $N_mF_2$ with $F_{107}$ are linear trend in equinoctial months,

saturation trend in June, and amplification trend in December respectively. Moreover, latitudinal differences are visible. Firstly, the establishments of the linear trend in equinoctial months and the amplification trend in December delay several hours in EIA crest region as compared with that at mid-latitude stations. Secondly, obvious decrease of $N_mF_2$ still continues after midnight at medium and high solar activity levels in EIA crest region in December, while $N_mF_2$ only changes little after midnight at mid-latitude stations.

[26] The possible mechanisms that cause these seasonal and latitudinal differences have been discussed. The conclusions can be drawn as follows:

[27] 1. Field-aligned plasma influx induced by the prereversal enhancement can significantly maintain $N_mF_2$, or even cause its increase, in EIA crest region at higher solar activity levels in equinoctial months and December. That causes the linear increase trend of $N_mF_2$ with $F_{107}$. And the continuous decrease of $N_mF_2$ at Okinawa in winter nights is also mainly due to higher $N_mF_2$ caused by the prereversal enhancement.

[28] 2. The recombination loss around the $F_2$-peak, which includes the effects of chemical and dynamic processes that cause the change of $h_mF_2$, induce the linear trend of $N_mF_2$ with $F_{107}$ developing to the amplification trend at Okinawa in December when field-aligned influx fades away. And it is dominant all the time at Okinawa in June. For mid-latitude station Wakkanai, the contribution of field-aligned influx to the solar activity variation trend of $N_mF_2$ is unconspicuous, the recombination loss around the $F_2$-peak is dominant.

[29] 3. There are greater values of $\beta_m$ at medium solar activity level in winter. That causes quicker recombination loss around the $F_2$-peak, which is responsible for the amplification trend in winter.

[30] We discussed the solar activity variations of both $h_mF_2$ and neutral atmosphere. It shows that both the solar activity variations of $h_mF_2$ and neutral parameters are important for the solar activity variation of nighttime $N_mF_2$. The variation trend of the recombination process around the $F_2$-peak is controlled by the relative increase intensities of $h_mF_2$ and neutral parameters. The result at Wakkanai shows that the sharper increase of neutral parameters (neutral temperature, density and vibrational excited $N_2$) with $F_{107}$ induces the enhanced recombination processes around the $F_2$-peak with $F_{107}$ in summer since the increase of $h_mF_2$ with $F_{107}$ is weaker as compared with that of recombination rate at higher altitudes. In contrast, there is a weaker response of neutral parameters to the variation of $F_{107}$ in winter, and the increase of $h_mF_2$ is more significant. But the reversal of neutral winds strongly lifts the $F_2$-peak to higher altitudes at low solar activity level, while there is no obvious change of $h_mF_2$ at high solar activity level due to a temporal delay of the reversal course. That induces quicker recombination processes around the $F_2$-peak at medium solar activity level, and causes the amplification trend of $N_mF_2$ with increasing $F_{107}$ in winter.

[31] **Acknowledgments.** The ionosonde data are provided by NICT, and $F_{107}$ data are taken from the SPIDR website. This research was supported by National Natural Science Foundation of China (40725014, 40674090) and National Important Basic Research Project (2006CB806306).

[32] Zuyin Pu thanks Dieter Bilitza and another reviewer for their assistance in evaluating this paper.

## References

Adler, N. O., A. G. Elias, and J. R. Manzano (1997), Solar cycle length variation: Its relation with ionospheric parameters, *J. Atmos. Sol. Terr. Phys.*, *59*(2), 159–162.

Balan, N., G. J. Bailey, B. Jenkins, P. B. Rao, and R. J. Moffett (1994a), Variations of ionospheric ionization and related solar fluxes during an intense solar cycle, *J. Geophys. Res.*, *99*, 2243–2253.

Balan, N., G. J. Bailey, and R. J. Moffett (1994b), Modeling studies of ionospheric variations during an intense solar cycle, *J. Geophys. Res.*, *99*, 17,467–17,475.

Balan, N., G. J. Bailey, and Y. Z. Su (1996), Variations of the ionosphere and related solar fluxes during solar cycles 21 and 22, *Adv. Space Res.*, *18*(3), 11–14.

Bilitza, D. (2001), International Reference Ionosphere 2000, *Radio Sci.*, *36*, 261–275.

Bilitza, D., V. Truhlik, P. Richards, T. Abe, and L. Triskova (2007), Solar cycle variations of mid-latitude electron density and temperature: Satellite measurements and model calculations, *Adv. Space Res.*, *39*, 779–789.

Buonsanto, M. J. (1990), Observed and calculated $F_2$ peak heights and derived meridional winds at mid-latitudes over a full solar cycle, *J. Atmos. Terr. Phys.*, *52*, 223–240.

Dudeney, J. R. (1983), The accuracy of simple methods for determining the height of the maximum electron concentration of the $F_2$-layer from scaled ionospheric characteristics, *J. Atmos. Terr. Phys.*, *45*, 629–640.

Fejer, B. G. (1981), The equatorial ionospheric electric fields: A review, *J. Atmos. Terr. Phys.*, *43*, 377–386.

Fejer, B. G., D. T. Farley, R. F. Woodman, and C. Calderon (1979), Dependence of equatorial F-region vertical drifts on season and solar cycle, *J. Geophys. Res.*, *84*, 5792–5796.

Fejer, B. G., E. R. de Paula, S. A. González, and R. F. Woodman (1991), Average vertical and zonal F region plasma drifts over Jicamarca, *J. Geophys. Res.*, *96*, 13,901–13,906.

Fejer, B. G., E. R. de Paula, R. A. Heelis, and W. B. Hanson (1995), Global equatorial ionospheric vertical plasma drifts measured by the AE-E satellite, *J. Geophys. Res.*, *100*, 5769–5776.

Gupta, J. K., and L. Singh (2001), Long term ionospheric electron content variations over Delhi, *Ann. Geophys.*, *18*, 1635–1644.

Hedin, A. E., et al. (1996), Empirical wind model for the upper, middle and lower atmosphere, *J. Atmos. Terr. Phys.*, *58*, 1421–1447.

Hierl, P. M., I. Dotan, J. V. seeley, J. M. Van Doren, R. A. Morris, and A. A. Viigiano (1997), Rates constants for the reactions of $O^+$ with $N_2$ and $O_2$ as a function of temperature (300–1800K), *J. Chem. Phys.*, *106*, 3540–3544.

Huang, Y., and K. Cheng (1995), Solar cycle variation of the total electron content around equatorial anomaly crest region in east Asia, *J. Atmos. Terr. Phys.*, *57*, 1503–1511.

Ivanov-Kholodny, G. S., and A. V. Mikhailov (1986), *The Prediction of Ionospheric Conditions*, 168 pp., Springer, New York.

Kane, R. P. (1992), Sunspots, solar radio noise, solar EUV and ionospheric $f_oF_2$, *J. Atoms. Terr. Phys.*, *54*, 463–466.

Kane, R. P. (2003), Solar EUV and ionospheric parameters: A brief assessment, *Adv. Space Res.*, *32*(9), 1713–1718.

Kawamura, S., N. Balan, Y. Otsuka, and S. Fukao (2002), Annual and semiannual variations of the midlatitude ionosphere under low solar activity, *J. Geophys. Res.*, *107*(A8), 1166, doi:10.1029/2001JA000267.

Kouris, S. S., P. A. Bradley, and P. Dominici (1998), Solar-cycle variation of the daily $f_oF_2$ and $M$ [3000]$F_2$, *Ann. Geophys.*, *16*, 1039–1042.

Lean, J. L., O. R. White, W. C. Livingston, and J. M. Picone (2001), Variability of a composite chromospheric irradiance index during the 11-year activity cycle and over longer time periods, *J. Geophys. Res.*, *106*, 10,645–10,658.

Lei, J., L. Liu, W. Wan, and S.-R. Zhang (2005), Variations of electron density based on long-term incoherent scatter radar and ionosonde measurements over Millstone Hill, *Radio Sci.*, *40*, RS2008, doi:10.1029/2004RS003106.

Liu, J. Y., Y. I. Chen, and J. S. Lin (2003), Statistical investigation of the saturation effect in the ionospheric foF2 versus sunspot, solar radio noise, and solar EUV radiation, *J. Geophys. Res.*, *108*(A2), 1067, doi:10.1029/2001JA007543.

Liu, L., W. Wan, and B. Ning (2004), Statistical modeling of ionospheric $f_oF2$ over Wuhan, *Radio Sci.*, *39*, RS2013, doi:10.1029/2003RS003005.

Liu, L., W. Wan, B. Ning, O. M. Pirog, and V. I. Kurkin (2006), Solar activity variations of the ionospheric peak electron density, *J. Geophys. Res.*, *111*, A08304, doi:10.1029/2006JA011598.

Liu, L., W. Wan, X. Yue, B. Zhao, B. Ning, and M.-L. Zhang (2007a), The dependence of plasma density in the topside ionosphere on the solar activity level, *Ann. Geophys.*, *25*, 1337–1343.

Liu, H., C. Stolle, M. Förster, and S. Watanabe (2007b), Solar activity dependence of the electron density in the equatorial anomaly regions observed by CHAMP, *J. Geophys. Res.*, *112*, A11311, doi:10.1029/2007JA012616.

Mikhailov, A. V., and V. V. Mikhailov (1995), Solar cycle variations of annual mean noon $f_oF_2$, *Adv. Space Res.*, *15*(2), 79–82.

Mikhailov, A. V., M. Förster, and T. Y. Leschinskaya (2000), On the mechanism of the post-midnight winter $N_mF_2$ enhancements: Dependence on solar activity, *Ann. Geophys.*, *18*, 1422–1434.

Pavlov, A. V. (1994), The role of vibrationally excited nitrogen in the formation of the mid-latitude negative ionospheric storms, *Ann. Geophys.*, *12*, 554–564.

Pavlov, A. V. (1998), New electron energy transfer rates for vibrational excitation of $N_2$, *Ann. Geophys.*, *16*, 176–182.

Pavlov, A. V., and M. J. Buonsanto (1996), Using steady state vibrational temperatures to model effects of $N_2$* on calculations of electron density, *J. Geophys. Res.*, *101*, 26,941–26,945.

Picone, J. M., A. E. Hedin, D. P. Drob, and A. C. Aikin (2002), NRLMSISE-00 empirical model of the atmosphere: Statistical comparisons and scientific issues, *J. Geophys. Res.*, *107*(A12), 1468, doi:10.1029/2002JA009430.

Richards, P. G. (2001), Seasonal and solar cycle variations of the ionospheric peak electron density: Comparison of measurement and models, *J. Geophys. Res.*, *106*, 12,803–12,819.

Richards, P. G., and D. G. Torr (1986), A factor of 2 reduction in the theoretical $F_2$ peak electron density due to enhanced vibrational excitation of $N_2$ in summer at solar maximum, *J. Geophys. Res.*, *91*, 11,331–11,336.

Rishbeth, H. (1986), On the $F_2$-layer continuity equation, *J. Atmos. Terr. Phys.*, *48*, 511–519.

Rishbeth, H. (1993), Day-to-day ionospheric variations in a period of high solar activity, *J. Atmos. Terr. Phys.*, *55*, 165–171.

Rishbeth, H., and O. K. Garriott (1969), *Introduction to Ionospheric Physics*, 331 pp., Elsevier, New York.

Rishbeth, H., S. Ganguly, and J. C. G. Walker (1978), Field-aligned and field-perpendicular velocities in the ionospheric $F_2$-layer, *J. Atmos. Terr. Phys.*, *40*, 767–784.

Scherliess, L., and B. G. Fejer (1999), Radar and satellite global equatorial F region vertical drift model, *J. Geophys. Res.*, *104*, 6829–6842.

Sethi, N. K., M. K. Goel, and K. K. Mahajan (2002), Solar cycle variations of $f_oF_2$ from IGY to 1990, *Ann. Geophys.*, *20*, 1677–1685.

St. Maurice, J. P., and D. G. Torr (1978), Nonthermal rate coefficients in the ionosphere: The reaction of $O^+$ with $N_2$, $O_2$ and NO, *J. Geophys. Res.*, *83*, 969–977.

Su, Y. Z., G. J. Bailey, and S. Fukao (1999), Altitude dependencies in the solar activity variations of the ionospheric electron density, *J. Geophys. Res.*, *104*, 14,879–14,891.

Whalen, J. A. (2004), Linear dependence of the postsunset equatorial anomaly electron density on solar flux and its relation to the maximum prereversal E × B drift velocity through its dependence on solar flux, *J. Geophys. Res.*, *109*, A07309, doi:10.1029/2004JA010528.

Y. Chen, H. Le, and L. Liu, Beijing National Observatory of Space Environment, Institute of Geology and Geophysics, Chinese Academy of Sciences, No. 19, Bei Tu Cheng West Road, Chao Yang District, Beijing 100029, China. (liul@mail.iggcas.ac.cn)